A numerical investigation of the effect of thermal aging, processing and humidity on initiation and delayed cracking in plasma-sprayed coatings

Bassem El Zoghbi, Rafael Estevez

▶ **To cite this version:**

Bassem El Zoghbi, Rafael Estevez. A numerical investigation of the effect of thermal aging, processing and humidity on initiation and delayed cracking in plasma-sprayed coatings. Surface and Coatings Technology, 2022, 438, pp.128379. 10.1016/j.surfcoat.2022.128379 . hal-04841756

HAL Id: hal-04841756
https://hal.science/hal-04841756v1

Submitted on 19 Dec 2024

HAL is a multi-disciplinary open access archive for the deposit and dissemination of scientific research documents, whether they are published or not. The documents may come from teaching and research institutions in France or abroad, or from public or private research centers.

L'archive ouverte pluridisciplinaire **HAL**, est destinée au dépôt et à la diffusion de documents scientifiques de niveau recherche, publiés ou non, émanant des établissements d'enseignement et de recherche français ou étrangers, des laboratoires publics ou privés.

Distributed under a Creative Commons Attribution - NonCommercial 4.0 International License

Version of Record: https://www.sciencedirect.com/science/article/pii/S0257897222003000
Manuscript_f4bab03c13d5a006e6ba407651558710

Surface & Coating Technologies

A numerical investigation of the effect of thermal aging, processing and humidity on initiation and delayed cracking in plasma-sprayed coatings

EL ZOGHBI,Bassem [1]

Faculty of Engineering, Lebanese University

Hadat Campus, Beirut, Lebanon

Bassem.elzoghbi@ul.edu.lb

ESTEVEZ,Rafael [2]

Laboratoire SIMaP, Science et Ingéniérie des Matériaux et Procédés

Université de Grenoble Alpes - CNRS UMR 5266

Phelma Campus, Bâtiment THERMO, 3ème étage

1130, rue de la piscine, B.P. 75 - F38402 Saint Martin d'Hères Cedex

Rafael.Estevez@univ-grenoble-alpes.fr

Abstract

[1] Assistant Professor at Lebanese University, Beirut, Lebanon
[2] Professor at Grenoble Alpes University, Saint Martin d'Hères Cedex, France

© 2022 published by Elsevier. This manuscript is made available under the CC BY NC user license
https://creativecommons.org/licenses/by-nc/4.0/

The effect of aging by the relaxation of the initial thermal stresses related to the processing on the initiation and propagation of the inter-splat and the intra-spat cracks in plasma sprayed zirconia is analyzed using finite element model and a description of failure with cohesive surfaces. A multi-scale approach is adopted in which the inter-splat and intra-splat crack growth is described with a rate- temperature and humidity dependent cohesive zone model that mechanically represents the reaction-rupture mechanism underlying stress and environmentally assisted sub-critical failure. It is found that the relaxation of the initial thermal stresses generates a significant initial damage at the inter-splat scale by the nucleation of inter-splat cracks and a minor initial damage at the intra-splat scale. The results show that the rate of inter-splat cracks increases with the relative humidity and especially with the temperature at which the relaxation occurs. The effect of the initial damage generated by the thermal aging on the resistance of the polycrystal of plasma sprayed zirconia against intra-splat slow crack growth under static fatigue loading is investigated. The results show that the initial damage at the intra-splat scale does not affect its resistance against intra-splat slow crack growth. However, the initial damage at the inter-splat scale leads to an increase in the slow cracking rate for a loading level K_I and a reduction in the threshold load K_0 below which no slow crack growth occurs as the individual splat is embedded in a damaged equivalent continuum representing the overall splat structure. The aim of this work is to provide a reliable predictions and insight in long lasting applications of plasma sprayed ceramic materials.

1. Introduction

Plasma sprayed ceramic coatings are widely used in engineering applications, such as thermal barrier coatings (TBC) to insulate components exposed at high temperature in advanced gas turbines. The processing of plasma sprayed ceramics consists in the injection of the ceramic powder particles that are melted and projected at high velocity toward substrate to form splats stacked perpendicular to the direction of the projection [1, 2]. The processing of plasma sprayed ceramics requires a cooling down about 1500K. During the solidification of a ceramic 'drop' onto the substrate, the solidified drop splits into several parts that results in the formation of the observed solid splats [3]. The coating then appears to be made of several layers of the splats, which also contains voids, and a grains-substructure within the splats can also be observed.

The micrographic observations show that the ceramic top coat has three scales:

i. the macroscale of the material involves a heterogeneous structure characterized by the existence of un-melted particles and large pores (actually originating from polishing induced large pits), of which size can be of the order of 100 microns [4] (see Fig. 1a). These features determine the overall strength of the material.

ii. the mesoscale corresponds to the sprayed splats that are formed during the solidification process of the melted ceramic particles. From the observations reported in [5], these splats can be schematically described as bricks with a diameter about 10 – 50 microns and 1 – 5 microns thick (See Fig. 1b) as in [6, 7] too. However, the thickness can vary with the processing and can be as small as 1 – 2 microns in the case of TBCs and

can appear larger in the case of well-bonded splats regions. These splats can also be separated by interlamellar pores resulting from rapid solidification and globular pores formed by incomplete inter-splat contact [8, 9].

iii. the microscale corresponds to the columnar micron grains with a diameter about 1 – 5 microns. This microstructure is comparable to that of ceramic polyccrystals produced by sintering. It could be considered as a 2D polycrystal (See Fig. 1c). that could lead to mainly two types of cracks in these coatings: the intra-splat cracks formed inside the splat along grain boundaries [10].

There are limited studies that aim to predict the influence of all aspects of the TBC microstructure on its failure behavior. Some studies have focused only on the effect of microstructural pores and have shown that pores greatly influence the effective properties of the material such as elastic moduli and thus their influence on failure in monotonic loadings but not those of slow crack growth (SCG) [6, 11]. However, the crack propagation studies show that inter- and intra-splats cracks contribute to a different fracture behavior of TBC materials [12, 13]. E. Wessel et al. [12] have studied the crack propagation in plasma sprayed thermal barrier coating subjected to four points bending tests. Their study shows a strong dependence of crack path and fracture toughness from pre-existing inter- and intra-splat cracks. These cracks may grow under certain mechanical and/or thermal loads and could lead to a delayed cracking of the material and then to a limit of the reliability over the long time. Therefore, the pre-existing inter- and intra-splat cracks should be taken into consideration in the analysis of the microstructural

aspects of crack growth and resistance within the TBC materials. L. Chen et al. [3] studied the primary formation mechanism for intra-splat cracking based on both experimental observations and mechanical analysis using a shear lag-model, assumed to be rate independent and considered some delamination between film and substrate too. Recently, N. Ferguen et al. [14] have modeled the crack propagation of plasma sprayed coatings subjected to uniaxial tension. The simulation results on crack propagation show that the generation of cracks initiates inside the splat from pre-existing intra-splat cracks. A.H. Bartlett et al. [15] studied the effect of heat treatment on failure mechanisms of Zirconia thermal barrier coating by performing a series of isothermal and cyclic heat treatments. The study shows that failure of plasma sprayed TBC initiates at the ceramic/bond coat interface and then propagate in the ceramic top coating itself.

Recently, G. Leclercq [5] studied the effect of aging on the thermomechanical behavior of Yttria-stabilized zirconia coating. The variation of the mechanical behavior and the mechanism of cracking were evidenced to be related to the aging program for specimens stored in different temperature and relative humidity (*R.H.*) of the climatic enclosure. The most severe aging condition was carried out at 134ºC and 100% of *R.H.* Water treatments between 3 days and 18 months depending on the storage conditions, lead to a reduction in the stress at rupture (40% - 50%) and in the elastic moduli (30% - 40%) over time. The microstructural observations have shown a significant increase about 15% in the crack density of the material by the propagation of inter-splat and intra-splat cracks. The evolution of crack propagation law of aged material was studied by performing static fatigue tests that result in SCG characterized by studying the variation of the crack velocity V under different load level K_I. The obtained results represented in

V-K_I plots have shown that increasing the time of aging induced a vertical/left shift in the V-K_I curve with an increase of crack velocity at a given load K_I (see Fig. 2b).

Therefore, it appears necessary to develop a numerical model, which is able to predict delayed cracking with a thermally activated crack growth, and assisted by the environment in order to understand the governing failure mechanisms at the level of the ceramic top coatings by taking into account the inter-splat and intra-splat structures.

M. Ortiz et al. [16] have examined the initiation of grain boundary micro-cracks related to thermal stresses in ceramic polycrystals under cooling with a finite element model. They have considered a large numbers of randomly oriented, planar hexagonal grains with a grain size range of 5 to 125 microns with elastic and thermal expansion anisotropy, and brittle grain interfaces, subjected to a uniform thermal load of –1500 Kelvins. They have shown that damage initiated by cooling is grain size dependent; the intergranular failure was observed for a grain size larger than a characteristic value about 5 microns for polycrystalline aluminum oxide. However, their model does not account for time-dependent rupture mechanisms, which is responsible for delayed cracking.

The aim of this work is to evaluate the effect of heat treatment and aging processes on the damage and possible failure of plasma sprayed zirconia. This is carried out by evaluating the initial damage of the material generated by the relaxation of the initial thermal stresses related to the processing. The crack propagation is described using a time-dependent, stress and environmentally dependent cohesive model that was shown able to capture SCG in ceramic polycrystals [17-20]. The adopted cohesive zone model mimics mechanically the reaction-rupture mechanism underlying stress and environmentally assisted failure. The cohesive parameters are identified from data for

SCG in zirconia single crystals which are assumed to be representative of inter-granular/inter-splat failure. Thus, depending on the scale under consideration, boundaries between splats or between grains in the inner splats are described with such cohesive surfaces. The influence of accelerated aging by increasing the temperature and *R.H.* on the initial damage generated by the relaxation of the initial thermal stresses is examined. Then, the influence of aging that promotes either inter-splat or intra-splat cracks under a constant mechanical load is evaluated. The paper is organized as follow: the next section 3 briefly presents the problem formulation and the adopted cohesive model is presented in section 4. Section 5 and 6 are devoted to the analysis of damage and failure at the meso-scale and micro-scale respectively. Section 7 presents a discussion on the results of this study and Section 8 concludes the paper.

2. Problem formulation

The microstructure of plasma sprayed zirconia is made of lamellar structure in form of splats with a diameter about 10 – 30 microns that appears as bricks pile up across the thickness [5, 6]. These splats are made from columnar grains with a diameter around 1 micron. The microstructure shows inter-splat cracks that lie along splat boundaries (see Fig 1b) and local cracks emerging from the edge of the splats (see Fig 1c). In this study, we investigate first the effect of processing by the relaxation of the initial thermal stresses on damage in terms of inter-splat and intra-splat crack at a given z-level of the thickness of the stack.

Secondly, the study addresses the case when the material is subjected to external loading, for example a bending loading (see Fig. 2a) then these cracks are subjected to mode I loading and could propagate. Even for loading levels below than toughness and

maintained constant with time, these cracks could propagate by SCG similar to the intergranular SCG observed in the sintering polycrystals of ceramics. However, the experimental results of SCG in polycrystal of ceramics show that increasing the grain size increases the material's resistance to SCG, while decreasing the velocity at a given load K_I and increasing of the threshold load K_0below which no SCG occurs (see Fig. 2b). In the case of plasma sprayed ceramics, the splats could be considered as grains with large grain size made of small columnar grains of diameter 1 micron. Therefore, the plasma sprayed materials are prone to intra-splat SCG when subjected to mechanical loading. Hence, when modeling intra-splat cracking between columnar grains, the microstructure is considered as 2D polycrystal represented by a granular zone immerged in an isotropic linear continuum representing the equivalent homogeneous medium. The failure mechanism is described within thermally activated cohesive zone methodology, which is presented in the following section.

3. Cohesive zone model for the description of the reaction-rupture mechanism

The initiation and propagation of inter-splat and intra-splat cracks in plasma sprayed zirconia is described with a thermally activated cohesive zone model. The formulation is initially proposed by Romero de la Osa et al. [17, 18] and employed by B. El Zoghbi et al. [19, 20] in order to predict the reaction-rupture mechanism underlying SCG in ceramic single crystal and polycrystals. The cohesive zone describes the reaction-rupture mechanism using a relation between the applied normal traction σ_n and the related opening of the cohesive surface Δ_n.

The formulation is based on a physical description of the reaction-rupture mechanism presented by T.A. Mischalske and S.W. Freiman [21] and revisited by T. Zhu

et al. [22] who demonstrated that the reaction rupture occurs when an energy barrier is overcome by thermal fluctuations once a stress threshold is reached locally, with an activation energy that decreases with the applied stress. Locally, the reaction-rupture mechanism is thermally activated, assisted by applied stress and the environment in terms of *R.H.* and temperature. Then, the failure process is thermally activated when the normal traction σ_n becomes higher than a local traction threshold σ_n^0 and it is described in a rate- and temperature-dependent cohesive model that is thermally activated. This is modeled with the proposed damage-opening rate between two cohesive surfaces as

$$\dot{\Delta}_n^c = \dot{\Delta}_0 \left(\frac{-U_0 + \beta \sigma_n}{k_B T} \right), \tag{1}$$

where U_0 is an activation energy, σ_n is the normal traction on the cohesive surface, $\dot{\Delta}_0$ is the pre-exponential term having the dimension of a velocity, β corresponds to an activation volume, T is the absolute temperature and k_B is the Boltzmann constant.

The relation (1) operates until the cumulated opening $\Delta_n^c = \int \dot{\Delta}_n^c \, dt$ reaches a critical extension Δ_n^{cr} corresponding to the nucleation of a crack locally.

When the rupture damage mechanism takes place, the traction-opening relationship is

$$\dot{\sigma}_n = k_n \left(\dot{\Delta}_n - \dot{\Delta}_n^c \right), \tag{2}$$

where $\dot{\sigma}_n$ is the normal traction increment, $\dot{\Delta}_n$ is the prescribed opening rate, $\dot{\Delta}_n^c$ is the reaction-rupture accommodation. The term k_n is a stiffness taken to be large enough to ensure that $\dot{\Delta}_n \approx \dot{\Delta}_n^c$ during the opening of the cohesive surface.

The normal opening mode is considered the only governing factor in the failure mechanism where a simple elastic response in tangential direction that is considered as

$$\dot{\sigma}_t = k_t \, \dot{\Delta}_t, \tag{3}$$

with $\dot{\sigma}_t$ is the tangential traction increment, $\dot{\Delta}_t$ represents the prescribed shear rate along the cohesive surface and k_t is the tangential stiffness. Practically, k_t is taken equal to k_n.

A quasi-static finite analysis is considered which uses a total Lagrangian description, the incremental shape of virtual work for this problem as [17-20]

$$\int_V \tau \delta \dot{\eta}\, dV + \int_{Scz} \sigma_\alpha \delta \dot{\Delta}_\alpha dS = \int_{\partial V} T \delta \dot{u} dS\,, \tag{4}$$

where V and ∂V respectively represent the volume of the region in the initial configuration and its boundary, and S_{CZ} is cohesive surface. The index α denotes the normal and tangential components in the cohesive formulation. In (Eq. 4), τ is the second Piola-Kirchhoff stress tensor, T the corresponding traction vector; $\dot{\eta}$ and $\dot{u}$ are respectively the conjugate Lagrangian strain rate and velocity. The governing equations are solved in a linear incremental fashion based on the rate form of (Eq. 4).

4. Influence of the initial thermal stresses and aging at splats' scale

In this section, the nucleation and growth of the inter-splat cracks in plasma sprayed zirconia due to the relaxation of the initial thermal stresses of processing are evaluated. To this end, we consider a set of splats at a given z-level in the thickness of the stack, each splat containing a set of columnar grains. Between two adjacent splats (see Fig. 3a), the columnar grains between two neighboring splats exhibit a crystallographic misorientation along the boundaries of the splats. We simplify this misorientation along the splats edges by considering a uniform crystallographic orientation for each splat (see Fig. 3b) in order to evaluate the influence of such orientation's mismatch on inter-splat

cracking. In addition, the splats are considered as hexagons with anisotropic (cubic) thermoelastic properties with random orientations. The corresponding mechanical properties are reported in Table 1. The splats have an anisotropic thermal expansion tensor, of which components are $\alpha_1 = \alpha_3 = 10 \times 10^{-6}\ \mathrm{K}^{-1}$ and $\alpha_2 = 11 \times 10^{-6}\ \mathrm{K}^{-1}$.

The inter-splat cracking is described with thermally activated cohesive surfaces that are inserted along the splats boundaries. The cohesive parameters have been identified from data for zirconia single crystal SCG [19, 20], of which values are borrowed to the present study and are reported in Table 2. According to T. Zhu et al. [22], a threshold stress σ_n^0 exists for the reaction-rupture to be energetically favorable, of which magnitude ranges from 0 to 30% of the athermal stress σ_c for breakdown. The athermal stress is $\sigma_c = \frac{U_0}{\beta} = 9615\ \mathrm{MPa}$ corresponds to a critical stress for the reaction-rupture to proceed in the absence of humidity at zero Kelvin. A threshold stress σ_n^0 = 400 MPa is considered, corresponding to 4% of the athermal stress σ_c, which is shown able to capture the minimum load level for the reaction-rupture to cease in the zirconia single crystal [19, 20]. Such "low" level of threshold stress σ_n^0 of the inter-splat reaction-rupture mechanism assumes that this latter is as easy or even easier to initiate inside a splat, considered as a 2D polycrystal. This is motivated from the expected weaker interface between splats compared to the grain-to-grain misorientation inside the splats.

Consequently, inter-splat cracking between the splats of the polycrystal is allowed. The considered microstructure consists in 15×15 hexagonal splats with a splat approximate diameter $\Phi_s = 16$ microns (see Fig. 4a and Fig. 4b).

In order to study the phenomenon of aging for ambient conditions by the relaxation of the initial thermal stresses related to the processing, we start by applying a cooling

temperature of which magnitude is $\Delta T = -1500$ K. The boundary conditions are reported in Fig. 4a. The stress component (σ_{yy}) distribution is reported in Fig. 4c, in which regions under tension and compression right after prescribing the cooling are observed. From this initial state, the relaxation of these initial thermal stresses are allowed by inter-splat cracking. After a relaxation time of 14 days, all cohesive elements exhibit a level of traction σ_n smaller than the threshold stress σ_n^0, so that stress relaxation by the reaction-rupture mechanism is no longer active.

The stress component (σ_{yy}) distribution after thermal relaxation is presented in Fig. 5(a). This corresponds to the cracking induced by the processing. The Positions (*X*-*Y*) of the nucleated cracks at different instants during relaxation are shown in Fig. 5b, where the colors represent the location of crack nucleation after 3seconds, 10 days and 14 days. The initial cracking kinetics take place in two characteristic stages. We observe an initiation of inter-splat cracks after an almost instantaneous relaxation time $t \approx 3$ seconds at different regions of the microstructure. The crack initiation begins at the regions with the highest initial stress concentrations (positive normal traction on the cohesive surfaces) take place. The paths of inter-splat cracks depend on the misorientation between the splats and the crack growth continues up to a maximum time of 14 days. The crack stops to propagate when it reaches a region in which the compression is initially high enough to result in a traction on the cohesive zone surfaces smaller than the threshold stress σ_n^0. The predicted initial cracking is in agreement with the predictions of M. Ortiz et al. [16] in the case of a 2D polycrystal subjected to a similar temperature cooling. They evidenced a critical grain size below which no cracking is observed, of the order of 5 microns.

According to M. Ortiz et al. [16], the inter-splats configuration ranges in the domain where some cracking is expected.

The influence of accelerated aging by increasing the *R.H.* and the temperature on the inter-splat cracking induced by the relaxation of the initial stresses resulting from the processing is investigated in the following sections.

4.1 Influence of accelerated aging by increasing the relative humidity on inter-splat cracking

In the previous section, we have observed that the microstructure of plasma spray zirconia at the splats scale is sensitive to initial cracking resulting from the processing with a cooling $\Delta T = -1500$ K. The aim of this section is to evaluate the influence of a larger *R.H.* on the initiation and growth of the inter-splat cracking induced by the relaxation of the initial thermal stresses. These conditions correspond to accelerated aging conditions that are considered to evaluate the material's durability or long lasting mechanical integrity. Increasing *R.H.* promotes further cracking by facilitating the reaction-rupture process. This is accounted for by reducing the magnitude of the "energy barrier" *U* in the expression of the cohesive opening rate (see Eq. 1). Inspired by the work of T. Zhu et al. [22], this is described with a dependence of the energy barrier U with *R.H.*, U decreasing with *R.H.*, thus increasing the damage opening rate $\dot{\Delta}_n^c$ for a given traction σ_n. In other words, an increase of *R.H.* results in decreasing the activation energy $U(R.H.)$ that facilitates the cracking. A reference activation energy $U_0 = 160\ \mathrm{kJ/mol}$ is considered for ambient conditions of which magnitude is derived from the sublimation

energy of technical ceramics [23]. A reduction of its value by 10% is shown sufficient in [19, 20] for promoting and acceleration of SCG under a larger *R.H.*

The patterns of the initial cracks nucleating during the relaxation of the initial thermal stresses are reported in Fig. 6. We observe that the increase of *R.H.* results to an increase in inter-splat cracking with respect to those observed for ambient conditions (See Fig. 5b). A larger number of inter-splat cracks are initiated after an almost instantaneous relaxation time $t \approx 3$seconds at different regions of the microstructure. For the reaction-rupture mechanism to cease, awaiting for a relaxation time of 10 hours is necessary compared to the 14 days necessary for ambient conditions. This is consistent with an accelerated process. Therefore, the initial damage and the associated cracking increase with increasing the local *R.H.*

The comparison of the final cracked splats structure for ambient conditions (Fig. 5b) and after "accelerated aging" by increasing *R.H.* shows that more cracks have nucleated for the accelerated conditions. This shows that increasing *R.H.* promotes cracking and it weakens the splat-to-splat boundaries. This is related to the description of the reaction-rupture that reduces the interface energy and the opening rate increases for a given traction, but also, reaching the conditions for failure can be attained for a lower local traction. Thus, aging by increasing *R.H.* is not only making the damage process faster, it also induced a reduction in the interface strength.

4.2 Influence of thermal aging on inter-splat cracking

In this section, the influence of thermal aging on the inter-splat cracks resulting from the relaxation of thermal stresses is investigated. In order to study the influence of

thermal aging, we simulate the relaxation of the initial thermal stresses in "a hot air" corresponding to a temperature $T = 393$ K. Then, a cooling $\Delta T = -1400$ K is considered instead of $\Delta T = -1500$ K in case of ambient conditions. The Positions $(X - Y)$ of the generated cracks are reported in Fig. 7. The cracks take place throughout the volume with a higher cracking rate than that generated by the relaxation of initial thermal stresses at ambient air (see Fig. 5b). We observe that the splats structure contains (much) more cracks, and also more cracks than in the case of *R.H*. aging (Fig. 6). This shows that the case under consideration here accelerates further the damage process and corresponds to a structure with even weaker interfaces to those reported for accelerated *R.H*. conditions. Again, increasing the temperature promotes damage, and not only its acceleration.

These results show that plasma sprayed zirconia is sensitive to thermal aging at the scale of splats. The thermal aging leads to an acceleration of damage opening rate $\dot{\Delta}_n^c$ although the magnitude of the initial level of the tensile and compressive thermal stresses is smaller. The influence of the damage rate appears dominant in the final damaged structure. Accelerated aging by increasing the temperature or *R.H* is not only a kinetic effect but involves a weakening of the splats boundaries, in the case considered here.

5. Effect of aging at the level of columnar submicron grains within a splat

The objective of this section is to evaluate and analyze the effect of thermal aging on the development of intra-splat cracking, inside a splat. Therefore, the plasma sprayed zirconia splat is modeled now at the microscale that corresponds to the columnar submicron grains. The intergranular cracking is considered only. This microstructure is comparable to that of ceramic polycrystals produced by sintering. All the splats

surrounding the considered columnar zone are represented by an equivalent homogeneous medium. Then, the intra-splat microstructure is considered as a granular zone composed by anisotropic hexagonal grains with random directions embedded in a homogeneous equivalent medium (see. Fig. 8a). The cubic elastic constants of zirconia grains are reported in Table 1 and the considered coefficients of thermal expansion are $\alpha_1 = \alpha_3 = 10 \times 10^{-6}\,\mathrm{K}^{-1}$ and $\alpha_2 = 11 \times 10^{-6}\,\mathrm{K}^{-1}$. The elastic properties of the surrounding homogenous linear isotropic bulk are extracted from the spherical and deviatoric parts of the cubic elastic moduli tensor from which the Young's modulus E^{iso} = 315 GPa and the Poisson ratio ν^{iso} = 0.24 are derived [24]. The thermal expansion of the surrounding bulk is $\alpha = \frac{2\alpha_1+\alpha_2}{3} = 10.3 \times 10^{-6}\,\mathrm{K}^{-1}$ in order to obtain an isotropic thermal response.

An initial crack emerges in the granular zone and cohesive surfaces are inserted along the columnar grain boundaries in order to simulate the propagation of intra-splat cracking (see Fig. 8). The cohesive parameters identified for a zirconia single crystal are again adopted [19, 20] (cf. Table 2). The granular zone consists in 8 × 8 grains with a grain diameter $\Phi_G = 0.8$ microns.

We consider a uniform cooling temperature $\Delta T = -1500$ K where the corresponding boundary conditions are presented in Fig. 8(a). The distributions of the corresponding stress component σ_{yy} are reported in Fig. 7(b) in which regions under tension and compression are observed due to the mechanical and thermal anisotropy of the grains and related misorientation in the granular zone. As a result, a pre-damage of the cohesive zones takes place in the regions for which the local traction normal to the surface under consideration is larger than the threshold stress σ_n^0. From this state, the relaxation of the

initial thermal stresses is allowed. If the level of stresses acting on the cohesive surfaces does not exceed the threshold stress σ_n^0 no cracking takes place. The value of the threshold stress σ_n^0 varies from 0 to 30% of the athermal stress σ_c. On other hand, the relaxation of the thermal stresses for different level of σ_n^0 shows that no cracking takes place for σ_n^0 level larger than 500 MPa. Thus, we consider a threshold stress $\sigma_n^0 = 400$ MPa that corresponds to 4% of the athermal stress σ_c. The distribution of the stress component (σ_{yy}) after relaxation of the initial thermal stresses is presented in Fig. 9a. The reaction-rupture continues to take place during a long duration about 540 days until the cease of the reaction-rupture when the levels of all stresses acting on the cohesive surfaces become smaller to σ_n^0. The Positions ($X - Y$) of the observed intra-splat cracks after the relaxation of the initial thermal stresses are reported in Fig. 9b. We observe that the initial intra-splat cracked zones are very localized compared to the size of the considered granular zone. This observation is thought to remain valid for other distribution of grain orientation, as this is thought to be random.

In next section, we investigate the influence of these initial intra-splat cracks on the prediction of intra-splat SCG by the application of a posterior static fatigue loading (constant remote load level).

5.1 Influence of the initial intra-splat cracks resulting from aging on the resistance of the polycrystal against intra-splat slow crack growth under static fatigue loading

In the previous section, we have considered the damage induced by the processing or aging at the intra-splat scale of plasma sprayed zirconia. In this section, we evaluate the

influence of these intra-splat cracks related to the processing on the prediction of intra-splat SCG under static fatigue loading, i.e. for a constant remote load level. The initial damaged state after the relaxation of the thermal stresses is presented in Fig. 9a. From this situation, an additional external load on the microstructure with initial cracks is considered. The prescribed loading is a mode I, and the K_I-displacement field is prescribed remotely, and "instantaneously" in order to prevent any damage induced when prescribing the target K_I. Thus an intra-splat intergranular failure is allowed. For example, the crack path in terms of the cracks positions $(X - Y)$ under a constant load $K_I = 1.89\ \mathrm{MPa}\sqrt{\mathrm{m}}$ is reported in Fig. 10a. We observe that the cracks trajectories are tortuous, resulting from the combination of the initial state of stress distribution and the grain-to-grain misorientation. However, the average cracks directions are close to the horizontal, as expected for a loading under mode I. Then, for each value of the applied load, the abscissa X of the crack advance with time is recorded and the corresponding crack velocity is calculated from a linear approximation of such propagation. By reducing the magnitude of the applied load K_I, a crack arrest is observed for a load threshold $K_0 = 1.89\ \mathrm{MPa}\sqrt{\mathrm{m}}$ of which crack pattern is presented in Fig. 10(b). The crack arrest is observed when the crack reaches a region where the compression is initially high enough to result in traction on the cohesive surfaces smaller than the threshold stress σ_n^0.

In order to evaluate the influence of the presence of initial intra-splat cracks, the predicted crack velocity V versus stress intensity factor K_I are reported in Fig. 11 and are compared to the results of intra-splat SCG without any initial damage for the same level of the threshold stress σ_n^0.

From these results, we observe that the damage induced by thermal aging at the intra-splat scale by the relaxation of the initial thermal stresses does not affect, neither the cracking kinetics, nor the load threshold level K_0 in the plasma sprayed zirconia subjected to a static fatigue loading. As the location of the initial cracks is away from the crack tip and related region of stress concentration, their presence does not influence the SCG dynamics and even related crack pattern. Therefore, with the ingredients considered in this section, aging would not influence the intra-splats SCG … is this so simple? This is further explored in the next section in which we evaluate the effect of the inter-splat damage caused by aging on the prediction of intra-splat SCG under static fatigue loading.

5.2 Influence of initial inter-splat damage related to the processing or aging on the resistance of the intra-splat slow crack growth

In the previous sections 5, we have observed that plasma sprayed zirconia splats structure is sensitive to cracking resulting from the relaxation of the initial thermal stresses under ambient conditions. The rate of inter-splat cracks increases with the *R.H.* and/or by increasing the temperature at which the relaxation takes place. The influence of this initial damage at the scale of the splats (see Fig. 1) on the intra-splat SCG along the columnar grains boundaries is now predicted by accounting for an equivalent homogeneous damaged medium at the splats scale (see Fig. 12).

When modelling intra-splat cracking between columnar grains, a 2D polycrystal is considered and represented by a granular zone embedded in an isotropic linear equivalent homogeneous medium (see Fig. 8a), representing the surrounding overall splats structure. However, the initial cracking resulting from hygrothermal aging appears important from

splat to splat and minor within the splats. Thus, we take into account the initial damage resulting from thermal aging by a reduction of the elastic moduli of the equivalent homogeneous medium.

Therefore, we consider the cases of initially damaged microstructure of which the Young modulus of the equivalent continuum decreases by 25% and 50% with respect to the reference value of undamaged medium $E^{ref} = 315\text{GPa}$. For each case of the Young's modulus of the equivalent homogeneous continuum, a cooling $\Delta T = -1500\text{K}$ is applied. Then the intra-splat SCG inside a splat between the columnar grains are evaluated by considering a 2D polycrystal made of 8 × 8 columnar grains with a grain diameter $\Phi_G = 0.8$ microns subjected to a static fatigue loading.

The results in terms of $V - K_I$ curves of intra-splat crack growth corresponding to the two "damaged" cases represented by a reduced moduli in the equivalent homogeneous medium, are presented in Fig. 13. These predicted SCG rates are compared with the results of intra-splat SCG obtained in the case of polycrystal of plasma sprayed zirconia without initial damage in the surrounding equivalent medium. For a given loading level K_I, we observe an increase in the kinetics of SCG and decrease in the level of the load threshold K_0 as the Young's modulus of the equivalent medium decreases.

These results show that the initial degradation of plasma sprayed zirconia at the splats scale related to thermal aging results in a reduction in the capacity of intra-splat crack growth resistance by increasing the crack velocity and decrease in the magnitude of load threshold K_0. This illustrates that the damage at these two scales needs to be considered simultaneously to gain insight on the durability of plasma spray microstructures.

6. Discussion

In this study, the microstructure of plasma spraying zirconia is considered at (i) the inter-splat scale and (ii) at intra-splat scale of columnar grains level. The splats are considered as hexagons. The splat-to-splat misorientation along the edges is taken into consideration in a simplified method with splats having a uniform crystallographic orientation. The thermal and mechanical anisotropy of splats was taken into account in a manner analogous to that of columnar grains. Thermally activated cohesive zones are inserted between splats to allow inter-splat cracking. The relaxation of the initial thermal stresses shows the nucleation of inter-splat cracks between splats generating a significant initial damage, resulting in a particular a reduction in the overall elastic moduli.

The influence of the accelerated aging by increasing the *R.H.* and the temperature on the inter-splat cracking induced by the relaxation of the initial thermal stresses is also evaluated. The results show that the amount of inter-splat cracks increase with the relative humidity and especially with the temperature at which the relaxation occurs. In addition, increasing simultaneously the temperature and the *R.H.* results in a more accelerated aging, not only the damage kinematics, but also a larger crack density and initial damage by inter-splat cracking.

The intra-splat scale is considered as a granular zone composed by anisotropic hexagonal grains with a random local orientation embedded in a continuum, homogeneous equivalent medium that represents the surrounding splats. The study of aging at the intra-splat scale shows modest cracking resulting from the relaxation of the initial thermal stresses. Then, the effect of these initial intra-splat cracks on the prediction

of the intra-splat SCG under static fatigue loading is investigated. For different load levels, the crack velocity is determined and the results are reported in $V - K_I$ curves and compared to that obtained without considering the relaxation of initial thermal stresses. The results show that the initial damage at the intra-splat scale does not affect its resistance against intra-splat SCG, as the principal crack does not interact with other preexisting flaws, those being too far from each other.

Eventually, the effect of the initial damage of the splats on the resistance of the material against intra-splat SCG between the columnar grains under static fatigue load is evaluated. To this end, we have considered the loading configuration with a granular zone embedded in an equivalent homogeneous damaged medium representing the damage in the pile-up of splats. Then, this initial damage of the equivalent homogeneous medium is considered by a reduction in its elastic moduli. A reduction in the equivalent Young's modulus E of the polycrystal of plasma sprayed zirconia subjected to static fatigue loading, results in an increase in the SCG rate for a loading level K_I and a reduction in the threshold level K_0 below which no slow crack propagation occurs. These results are in agreement with the experimental results of G. Leclercq [5] in the effect of aging on SCG of plasma sprayed zirconia that show a shift in the V-K_I curve with an increase of crack velocity at a given load K_I.

7. Conclusion

This work presents a finite element methodology for modeling the initiation and propagation of inter-splat and intra-splat cracks in the zirconia top coats of plasma sprayed zirconia. The mechanism underlying failure is described with thermally activated

cohesive zone methodology that represents the reaction-rupture process for SCG. The effect of aging by the relaxation of the initial thermal stresses of processing on the nucleation and propagation of the inter-splat and intra-splat is evaluated. Then, the effect of accelerated aging by increasing the temperature and the *R.H.* on either inter-splat or intra-splat cracking is examined and analyzed in details. In addition, the evolution of SCG behavior of the aged materials is evaluated. The main conclusions are as follows:

- The relaxation of the initial thermal stresses of processing generates a significant initial damage by the nucleation of inter-splat cracks between splats and minor intra-splat cracks that corresponds to the intergranular cracking inside splats.
    - Accelerated aging by increasing the *R.H.* and/or the temperature increases the inter-splat crack density and their nucleation rate and involves a weakening of the splats boundaries.
    - The resistance of aged plasma spraying zirconia against SCG considered by a reduction in the equivalent Young's modulus E of the polycrystal shows an increasing of crack velocity for a given load and an increasing of the threshold load level.

Such predictions and insight can only be accessible by a local approach of fracture.

REFERENCES

[1] R.A. Miller, J. Therm. Spray Technol. 6 (1997) 35–42.

[2] T. Clyne, S. Gill, J. Therm. Spray Technol. 5 (1996) 401.

[3] L. Chen, G.-J. Yang, C.-X. Li, C.-J. Li, J. Therm. Spray Technol. 25 (2016) 959–970.

[4] B. Siebert, C. Funke, R. Vassen, D. Stover, J. Mater. Process. Technol. 93 (1999) 217–223.

[5] G. Leclercq, Ph.D. dissertation, INSA Lyon, (2014).

[6] T. Nakamura, G. Qian, C.C. Berndt, J. Am. Ceram. Soc. 83 (2000) 578–584.

[7] G. Montavon, S. Sampath, C. Berndt, H. Herman, C. Coddet, J. Therm. Spray Technol. 4 (1995) 67–74.

[8] A. Kulkarni, Z. Wang, T. Nakamura, S. Sampath, A. Goland, H. Herman, J. Allen, J. Ilavsky, G. Long, J. Frahm, R.W. Steinbrech, Acta Materialia 51 (2003) 2457-2475.

[9] L. Chen, G.J. Yang, J. Adv. Ceram. 7 (2018) 17–29.

[10] H. Herman, Sci. Am. (1988) 112–117.

[11] Y. Wang, R. Gauvin, M. Kong, C. Lin, Z. Liu, Y. Zeng, Surf. Coat. Technol. 316 (2017) 239-245.

[12] E. Wessel, R. Steinbech, Key Eng. Mater. 223 (2002) 55.

[13] R. Sobhanverdi, A. Akbari, Ceram. Int. 41 (2015) 14517–14528.

[14] N. Ferguen, Y. Mebdoua-Lahmar, H. Lahmar, W. Leclerc, M. Guessasma, Surf. Coat. Technol. 371 (2019) 287–297.

[15] A.H. Bartlett, R.D. Maschio, J. Am. Ceram. Soc. 78 (1995) 1018-1024.

[16] M. Ortiz, S. Suresh, ASME J. Appl. Mech. 60 (1993) 77-84.

[17] M. Romero de la Osa, R. Estevez, J. Chevalier, C. Olagnon, Y. Charles, L. Vignoud, C. Tallaron, Int. J. Fract. 158 (2009)157–167.

[18] M. Romero de la Osa, R. Estevez, J. Chevalier, C. Olagnon, Y. Charles, L. Vignoud and C. Tallaron, Modell. Simul. Mater. Sci. Eng. 19 (2011) 074009.

[19] B. El Zoghbi, R. Estevez, C. Olagnon, Theor. Appl. Mech. 3 (2013) 051001

[20] B. EL Zoghbi, R. Estevez, Strength Fract. Complex.12 (2019) 15 – 30

[21] T.A. Michalske, S.W. Freiman, J. Am. Ceram. Soc. 66 (1983) 284–288.

[22] T. Zhu, J. Li, X. Lin, S. Yip, J. Mech. Phys. Solids. 53 (2005) 1597–1623.

[23] S.N. Zhurkov, Int. J. Fract. 26 (1984) 295–307.

[24] I. Doghri, A. Ouaar, Int. J. Solids Struct. 40 (2003) 1681–1712.

[25] J. Li, H. Liao, X. Wang, C. Coddet, J. Am. Cer. Soc., 86 (2003) 1906-10

Figure Captions List

Fig. 1 Diagram showing the three scales of plasma sprayed ceramics.

Fig. 2 Schematic description of the microstructure of plasma sprayed ceramics subjected to bending loading b) Schematic description of SCG in terms of crack velocity versus load level K_I.

Fig. 3 Schematic representation of the configuration used to model the microstructure of plasma sprayed ceramics at the splats scale. The splats are made up of anisotropic grains with random orientations.

Fig. 4 (a) Mesh and boundary conditions applied for the thermal loading of a plasma sprayed zirconia on the scale of splats, the microstructure is made of 15 × 15 splats with a splat size Φ_s = 16 μm, (b) Generation of hexagonal splat, (c)stress component (σ_{yy}) distribution after a cooling ΔT = -1500 K..

Fig. 5 (a) Stress component (σ_{yy}) distribution after a relaxation of initial thermal stresses for a relaxation period of 14 days. (b) Positions ($X - Y$) of inter-splat cracks between splats due to the relaxation of the initial thermal stresses of processing.

Fig. 6 Positions ($X - Y$) of inter-splat cracks between splats representing the influence of *R.H.* with a dependence of the activation energy U (*R.H.*). The increase in the local water concentration promotes inter-splat cracking of plasma sprayed zirconia.

Fig. 7 Influence of thermal aging on inter-splat cracking in plasma sprayed

zirconia. The inter-splat cracking rate is significantly higher than that observed under ambient temperature.

Fig. 8 (a) Boundary conditions for thermal load. (b) Distribution of the stress component σ_{yy} in the polycrystal of zirconia with Φ_G = 0.8 μm after a thermal cooling ΔT = -1500 K.

Fig. 9 Relaxation of initial thermal stresses of processing for a duration of 540 days and for a threshold stress σ_n^0= 400 MPa. a)) stress component (σ_{yy}) distribution after relaxation, b) Positions ($X - Y$) of the observed intra-splat cracks after the relaxation of the initial thermal stresses

Fig. 10 a) Crack path corresponding to the load K_I = 1.89 MPa$\sqrt{m}$, b) Crack path for stopped crack corresponding to the load threshold K_0 = 0.79 MPa$\sqrt{m}$.

Fig. 11 Comparison of the intra-splat SCG plots $V - K_I$ between plasma sprayed zirconia subjected to thermal aging by the relaxation of initial thermal stresses at the scale of intra-splat grains and without considering the relaxation of the initial thermal stresses.

Fig. 12 Schematic description of the microstructure of plasma sprayed zirconia with two characteristic length scales, (i) the stacking of splats, (ii) the intra-splat columnar structure.

Fig. 13 $V - K_I$ curves representing the influence of the initial damage of the isotropic continuum represented by a reduction of its Young's modulus, on the intra-splat crack growth resistance in plasma sprayed zirconia.

Table Caption List

Table 1 Cubic elastic constants of zirconia grains [19, 20].

Table 2 Cohesive zone parameters for SCG in zirconia single crystal [19, 20].

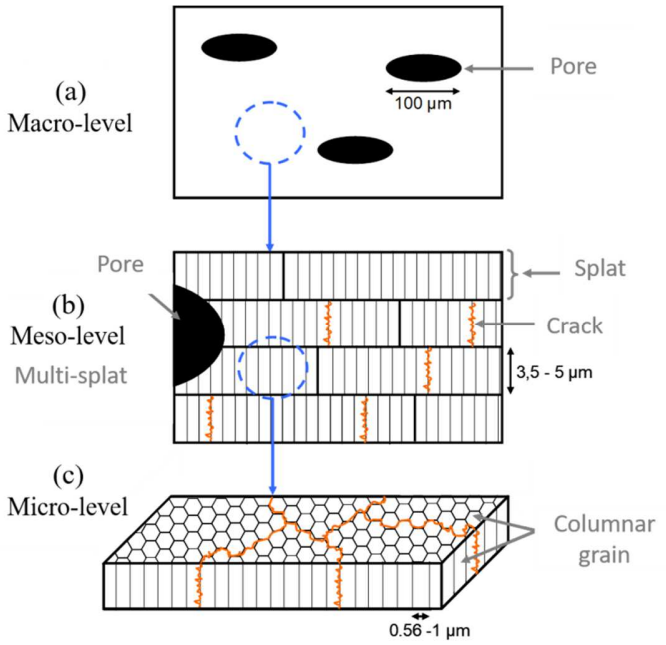

Fig. 1 Diagram showing the three scales of plasma sprayed ceramics.

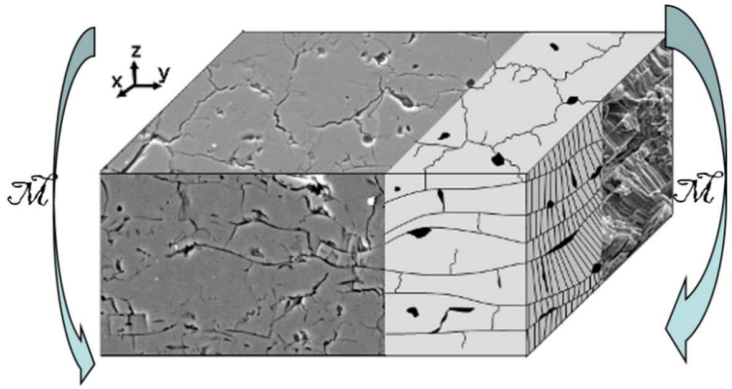

(a)

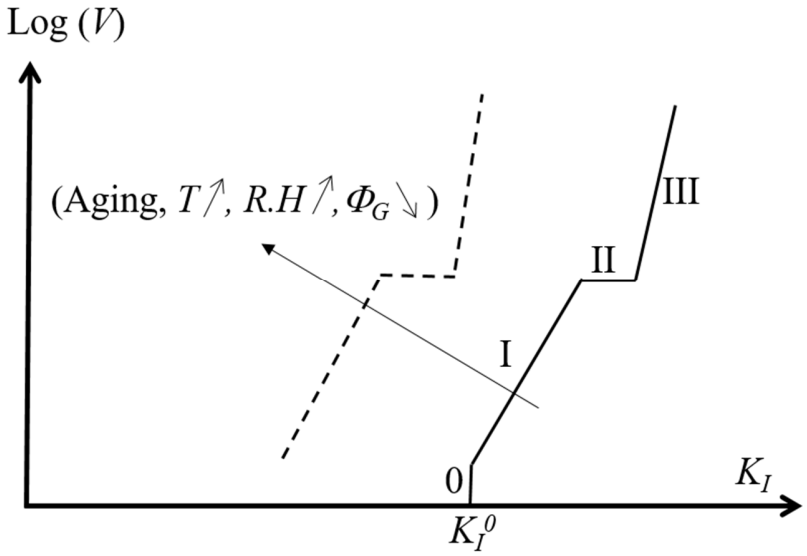

(b)

Fig. 2 Schematic description of the microstructure of plasma sprayed ceramics subjected to bending loading. b) Schematic description of SCG in terms of crack velocity versus load level K_I .

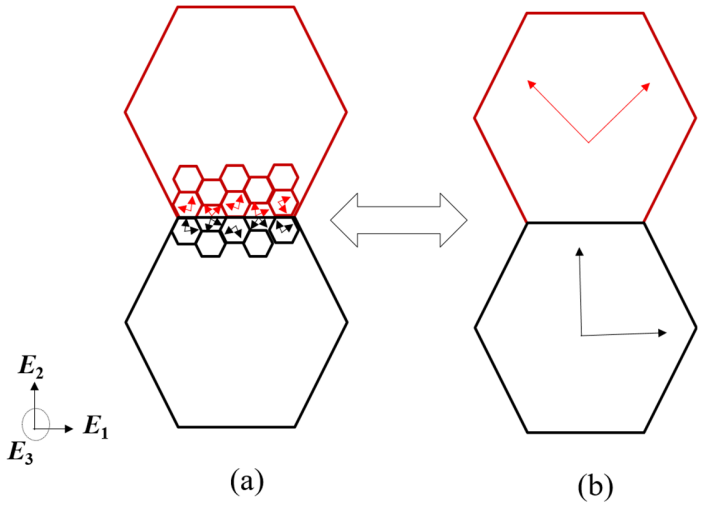

Fig. 3 Schematic representation of the configuration used to model the microstructure of plasma sprayed ceramics at the splats scale. The splats are made up of anisotropic grains with random orientations.

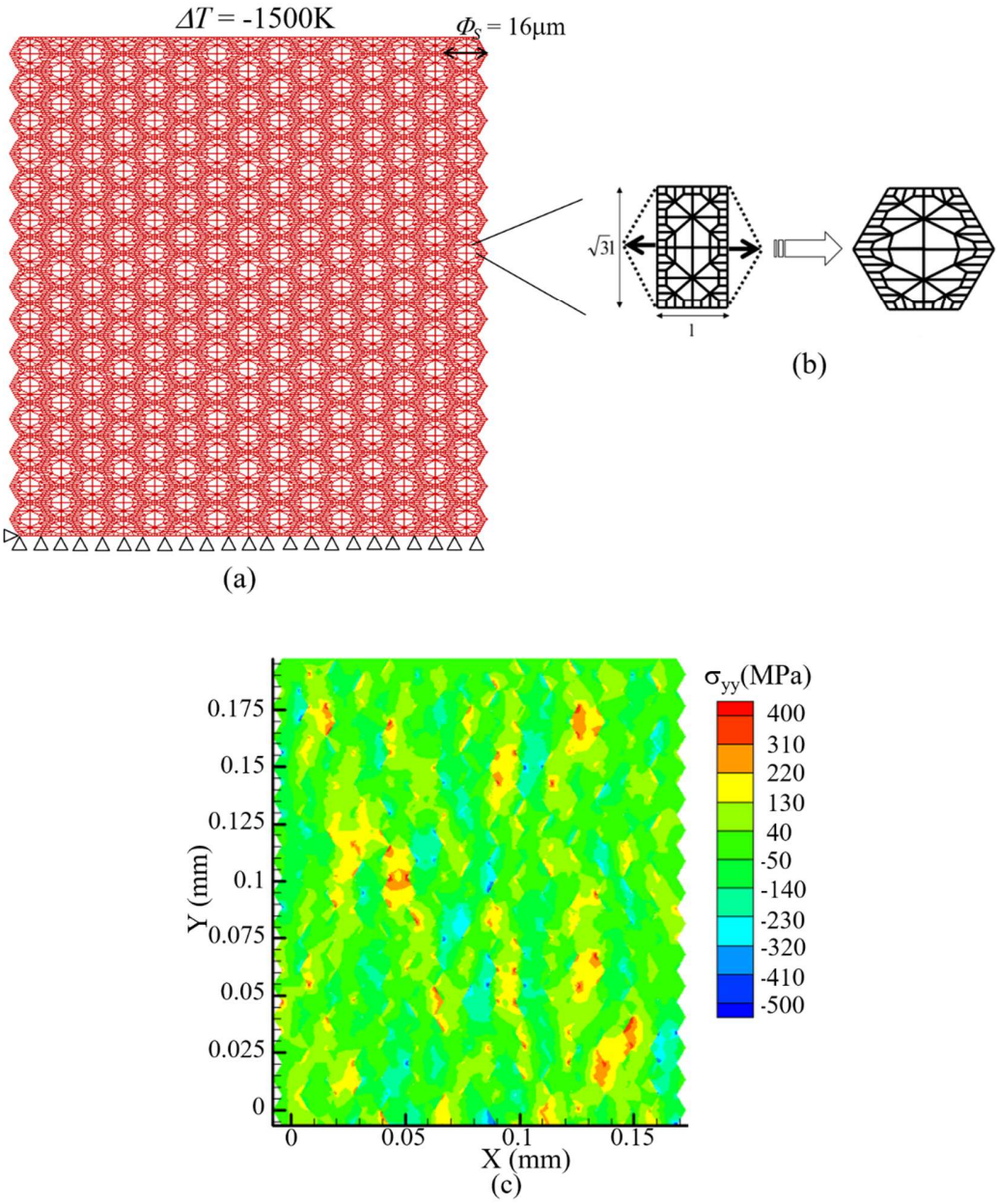

Fig. 4 (a) Mesh and boundary conditions applied for the thermal loading of a plasma sprayed zirconia on the scale of splats, the microstructure is made of 15 × 15 splats with a splat size Φ_s = 16 μm, (b) Generation of hexagonal splat, (c)stress component (σ_{yy}) distribution after a cooling ΔT = -1500 K..

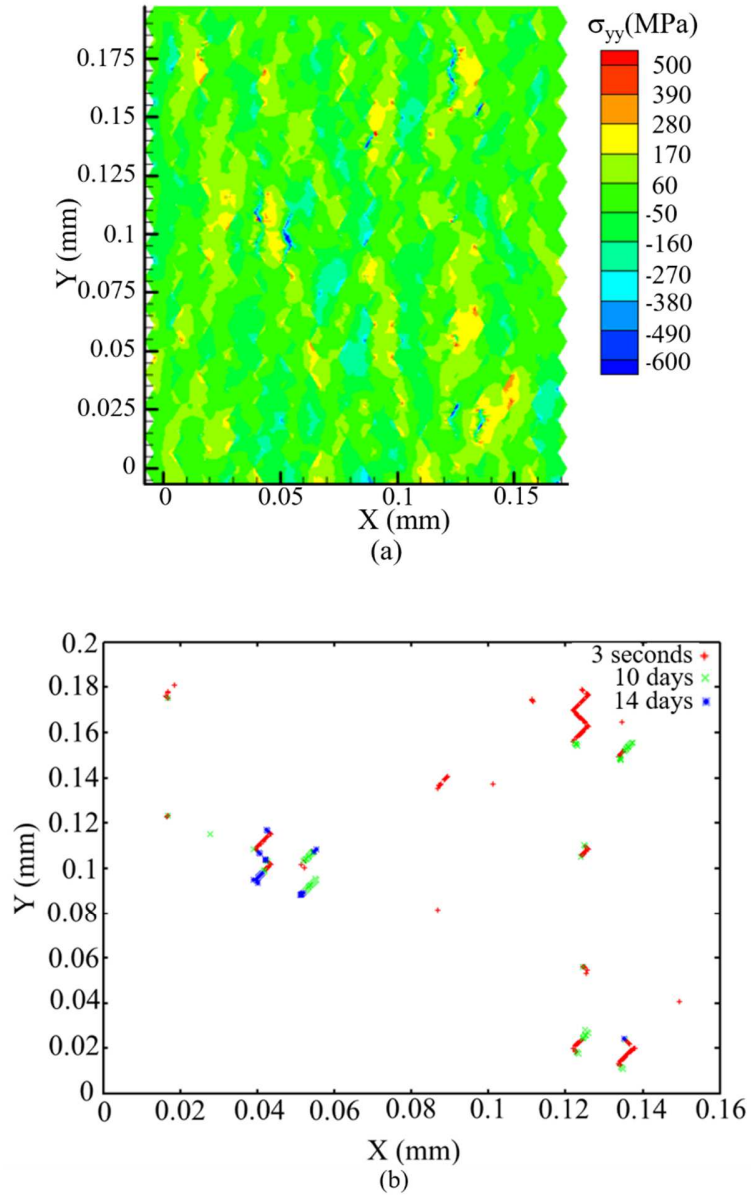

Fig. 5 (a) Stress component (σ_{yy}) distribution after a relaxation of initial thermal stresses for a relaxation period of 14 days. (b) Positions ($X - Y$) of inter-splat cracks between splats due to the relaxation of the initial thermal stresses of processing.

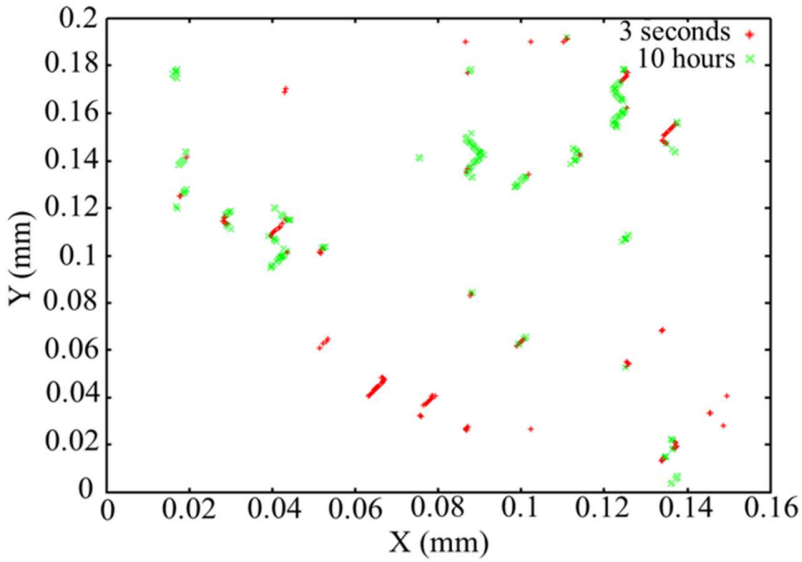

Fig. 6 Positions ($X-Y$) of inter-splat cracks between splats representing the influence of *R.H.* with a dependence of the activation energy U ($R.H$). The increase in the local water concentration promotes inter-splat cracking of plasma sprayed zirconia.

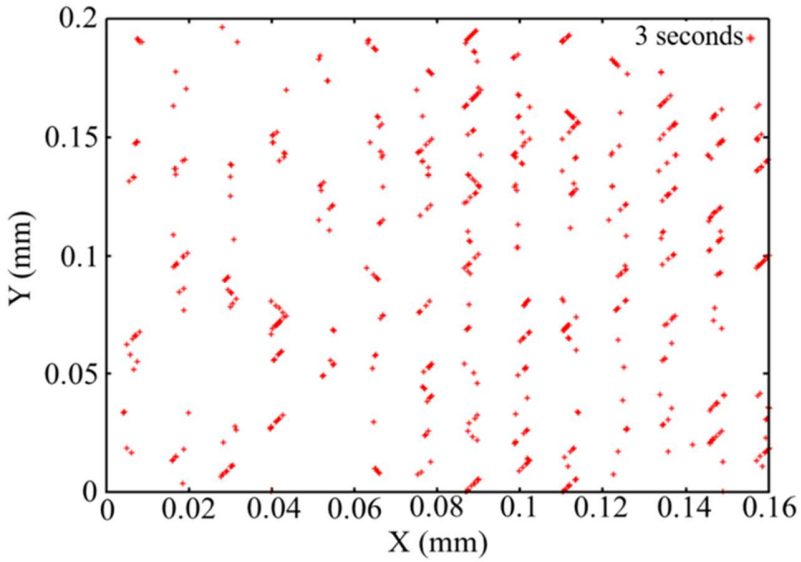

Fig. 7 Influence of thermal aging on inter-splat cracking in plasma sprayed zirconia. The inter-splat cracking rate is significantly higher than that observed under ambient temperature.

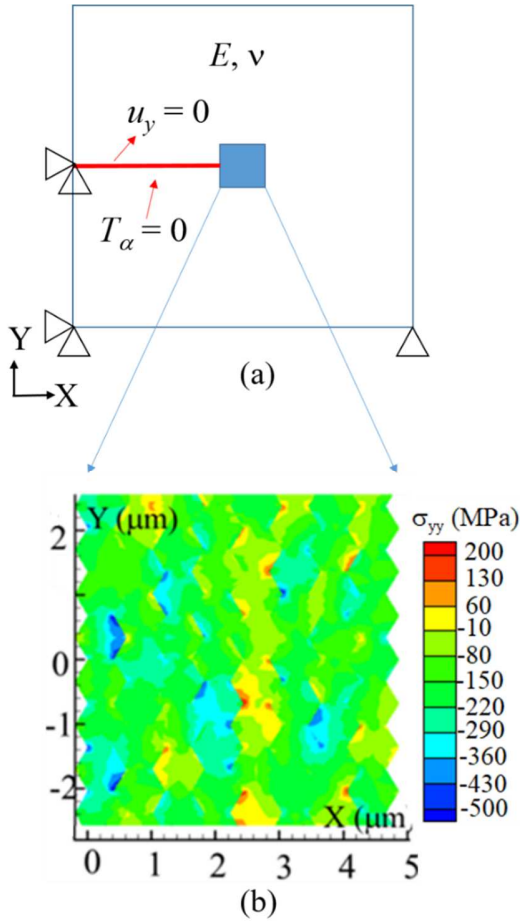

Fig. 8 (a) Boundary conditions for thermal load. (b) Distribution of the stress component σ_{yy} in the polycrystal of zirconia with Φ_G = 0.8 μm after a thermal cooling ΔT = -1500 K.

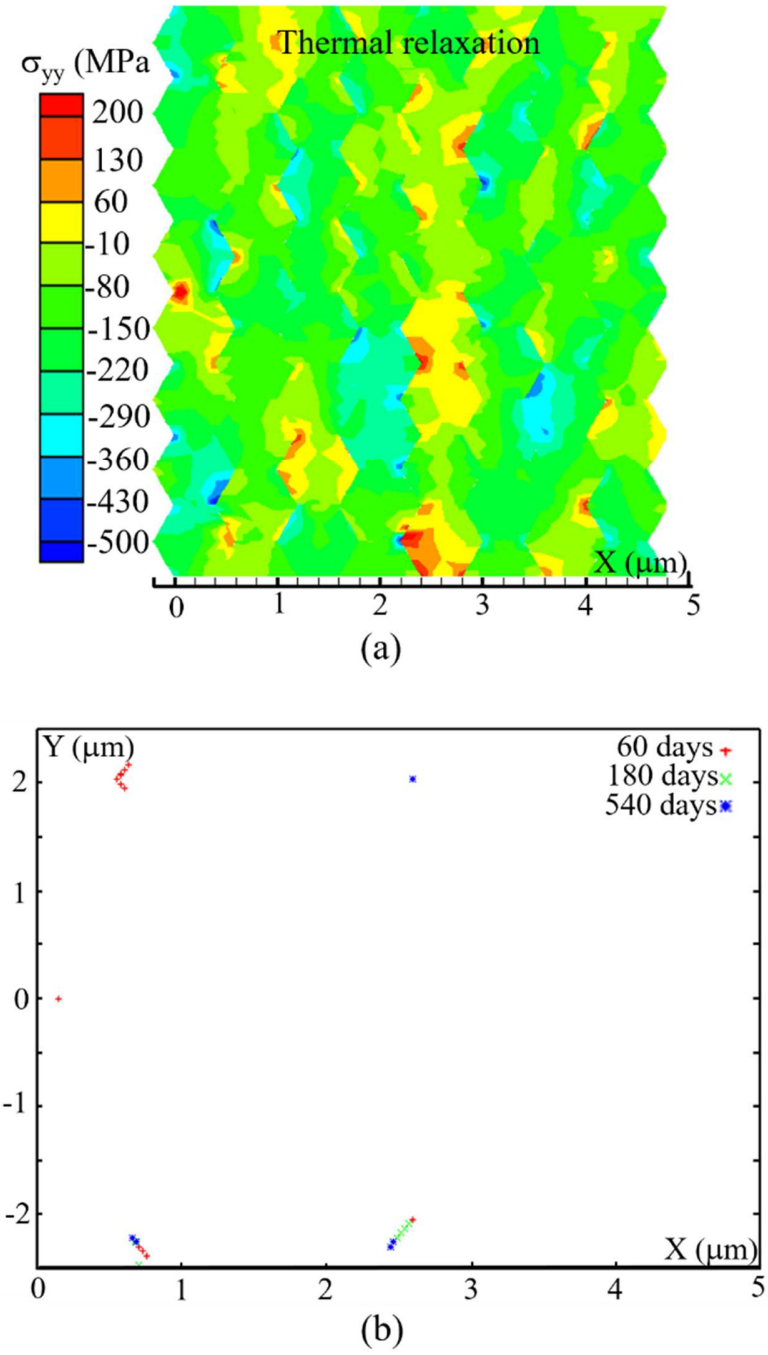

Fig. 9 Relaxation of initial thermal stresses of processing for a duration of 540 days and afor a threshold stress σ_n^0= 400 MPa. a)) stress component (σ_{yy}) distribution after relaxation, b) Positions ($X - Y$) of the observed intra-splat cracks after the relaxation of the initial thermal stresses.

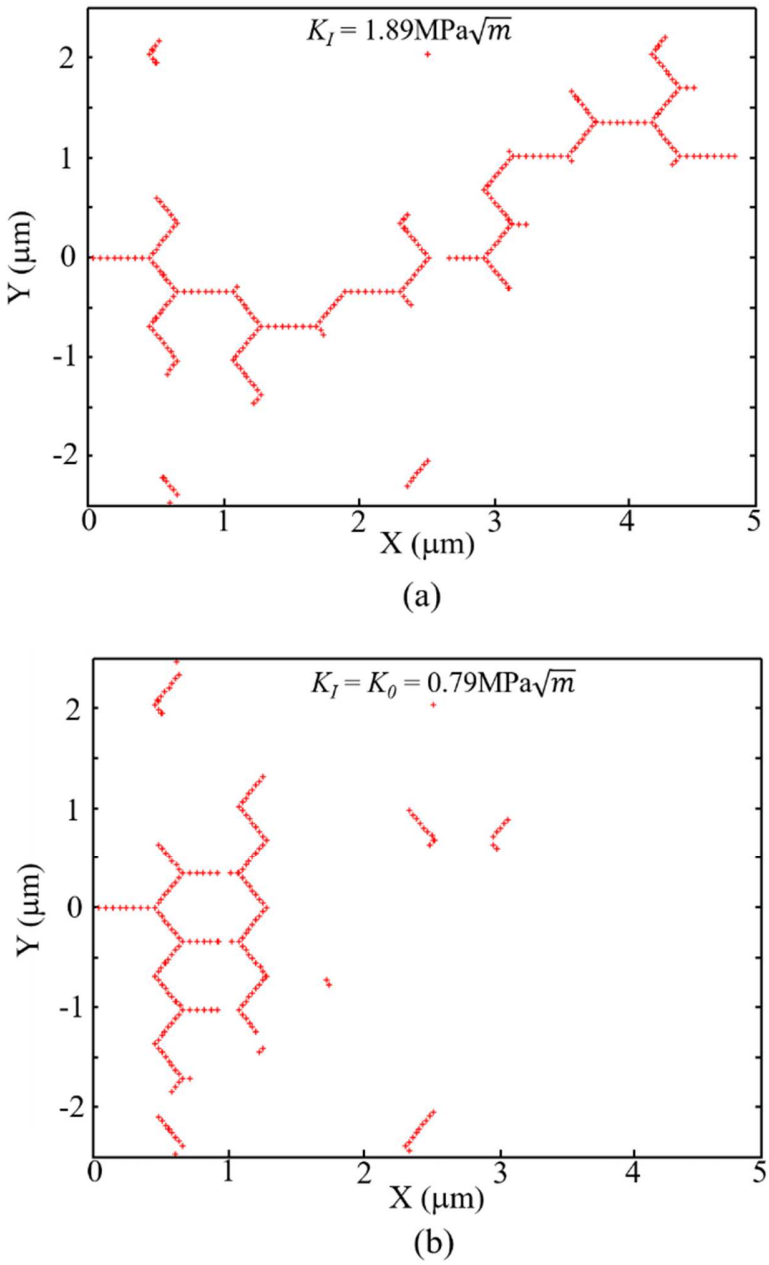

Fig. 10 a) Crack path corresponding to the load K_I = 1.89 MPa$\sqrt{\text{m}}$, b) Crack path for stopped crack corresponding to the load threshold K_0 = 0.79 MPa$\sqrt{\text{m}}$.

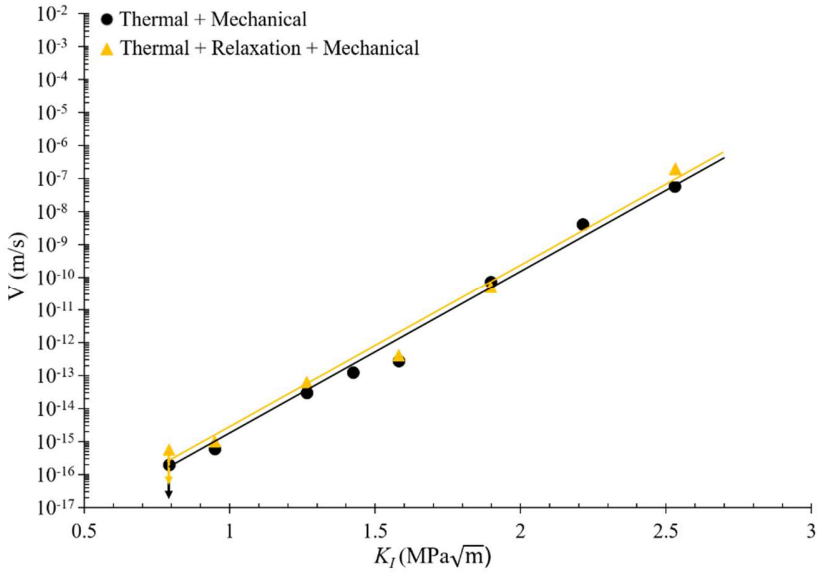

Fig. 11 Comparison of the intra-splat SCG plots $V - K_I$ between plasma sprayed zirconia subjected to thermal aging by the relaxation of initial thermal stresses at the scale of intra-splat grains and without considering the relaxation of the initial thermal stresses.

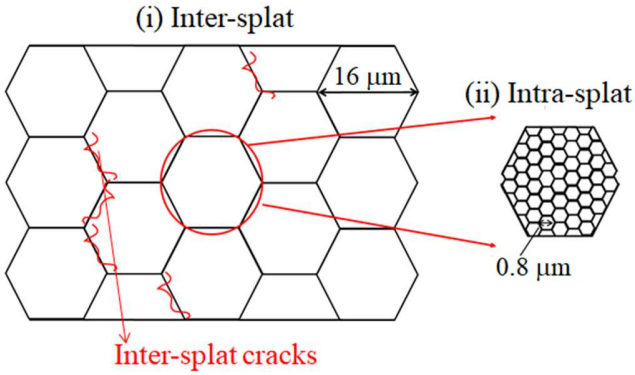

Fig. 12 Schematic description of the microstructure of plasma sprayed zirconia with two characteristic length scales, (i) the stacking of splats, (ii) the intra-splat columnar structure.

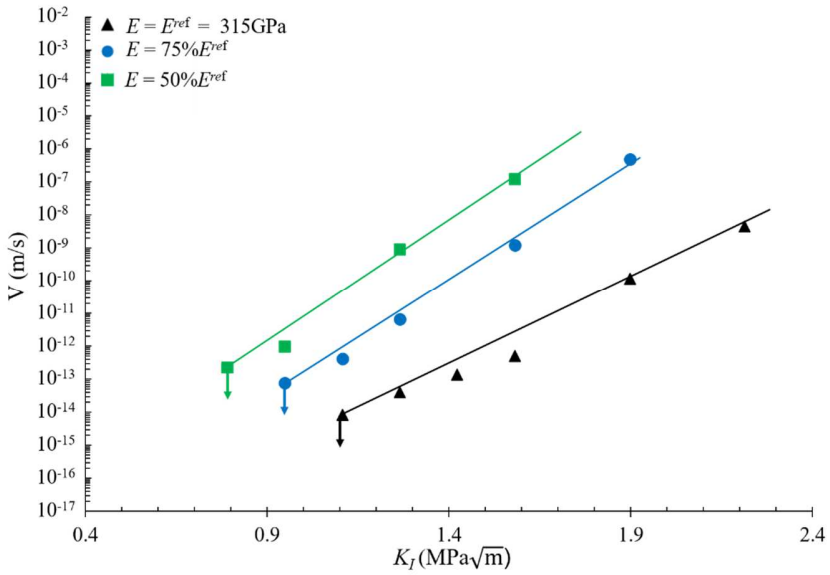

Fig. 13 $V - K_I$ curves representing the influence of the initial damage of the isotropic continuum represented by a reduction of its Young's modulus, on the intra-splat crack growth resistance in plasma sprayed zirconia.

Table 1. Cubic elastic constants of zirconia grains [19, 20].

L_{11}(GPa)	L_{22}(GPa)	L_{33}(GPa)
430	94	64

Table 2. Cohesive zone parameters for SCG in zirconia single crystal [19, 20].

U_0 (kJ/mol)	Δ_n^{cr} (mm)	β nm^3	$\dot{\Delta}_0$ (mm/s)
160	1	0.027	3.2×10^{11}